

## Biosynthesis zinc oxide nanoparticles using *Apium graveolens* L. leaf extract and its use in removing the organic pollutants in water

Himdad Hamad Azeez<sup>a,\*</sup>, Azeez Abdullah Barzinjy<sup>a,b,\*</sup>

<sup>a</sup>Department of Physics, College of Education, Salahaddin University-Erbil, Kurdistan Region, Iraq

<sup>b</sup>Department of Physics Education, Faculty of Education, Tishk International University, Erbil, Kurdistan Region, Iraq, Tel. 009647504542010; emails: himdad.azeez@su.edu.krd (H.H. Azeez), azeez.azeez@su.edu.krd (A.A. Barzinjy)

Received 19 September 2019; Accepted 9 February 2020

### ABSTRACT

This study consists of a reliable process for synthesizing ZnO NPs by green method. Here, *Apium graveolens* L. leaf extract is utilized as an efficient chelating and capping agent. The plant ingredients, structure, morphology, thermal behavior, chemical composition, and optical properties of ZnO nanoparticles were investigated using several characterization techniques, namely X-ray diffraction (XRD), field emission scanning electron microscopy, energy-dispersive X-ray spectroscopy, high-resolution transmission electron microscope (HRTEM), differential scanning calorimetry (DSC) analysis, Fourier transform infrared (FTIR) analysis, and UV-visible (UV-Vis) spectroscopy. The UV-Vis and FTIR analysis of *A. graveolens* L. leaf extract verified that this extract is a promising candidate for biosynthesizing ZnO NPs. The XRD spectrum, HRTEM, and the scanning electron microscope images confirmed the crystallinity and the spherical-shape of the ZnO NPs with an average size between 30 and 35 nm. The band-gap of the ZnO were measured to be around 3.132 eV. DSC analysis exhibits two endothermic peaks related to the water evaporation absorbed by the NPs and modification of zinc complex to zinc hydroxide, with a single exothermic peak related to the crystallization of ZnO NPs and degradation of organic materials. The ZnO NPs was employed for removing organic pollutants, that is, methyl orange (MO) from water using UV-Vis spectroscopy. Nearly an entire degradation of MO was achieved within 3 min of UV light radiation.

**Keywords:** Biosynthesis method of NPs; ZnO NPs, *Apium graveolens* L.; MO degradation; Water treatment

### 1. Introduction

Nanoparticles display new characteristics which vary considerably from those shown by their bulk material equivalents due to their extremely tiny sizes, that is, order of  $10^{-9}$  m. Their tiny dimensions provide them extraordinary surface-to-volume ratios which permit them to confine electron motions inside boundaries associated with improving the optical properties. This makes them particularly desirable in various areas such as medicine [1], drug delivery [2], water purification [3], agriculture [4], food [5], solar cells [6], cosmetics [7], textiles [8], and electronics [9].

Metals and metal oxides nanomaterial exhibit important physicochemical properties which include higher conductivity, catalytic activity; unusual optical properties and pyro-mechanical properties. They also have antimicrobial activity against pathogenic microorganisms [10–13]. Concerning the biological activity of nanoparticles, it has been shown that silver (Ag NPs) and zinc oxide (ZnO NPs) have an inhibitory effect on the growth of bacterial and fungal strains, when used in concentrations comparable to those used in antibiotics to treat infectious diseases [14,15].

It has been proven that metal nanoparticles, despite offering antimicrobial activity, could exhibit cytotoxic effects

\* Corresponding authors.

on healthy and carcinogenic cell lines, depending on the concentration used [16,17]. In addition, it has been indicated that the stability of nanoparticles is endangered in physiological conditions since the presence of biological compounds such as enzymes can delay the effective action of nanoparticles at the site of infection.

Nowadays, various physical, chemical, biological, and hybrid approaches are applied effectively in the production of different types of inorganic NPs, nevertheless they are pricey and need the usage of damaging chemical substances. Therefore, our environment is suffering from harm and an enormous quantity of unwanted materials [18]. For the time being, we need to discover the paradoxes that may exist in nature for alternative plans. In this manner, we will be able to deal with environmentally friendly and repairable materials, and completely away from using toxic materials. These novel spotless skills can extremely decrease ecological pollution and decline the danger to human healthiness as a result of utilizing harmful chemicals and solvents [19]. On the other hand, producing nanoparticles from physical and chemical approaches, with various dimensions and shapes, require stabilizing agents since in most cases they are unsteady [20].

Biosynthesized NPs from plant extracts are, usually, prepared from biological part of plants. Plant parts, for instance leaf, root, stem, and seed, are widely utilized for synthesizing metal-based NPs. Moreover, plant extracts contain bioactive polyphenols, alkaloids, proteins, sugars, phenolic acids, terpenoids, etc., they play a significant role in reducing the metallic ions and later stabilizing them [21].

In order to solve the difficulties involved in the use of nanoparticles as antimicrobial agents, encapsulation of metal nanoparticles has been proposed as a strategy that would reduce the possible cytotoxic effect, improve stability and increase bioavailability. Thus, the degradation would be avoided, and therefore the circulation time would be increased allowing a controlled release of the active agent. Fig. 1 displays the grouping of dissimilar NP production methods.

The biosynthesis of plant mediated nanoparticles can be classified into three phases: reduction phase, growth phase,

and stabilization phase [22]. The reduction phase is the most important phase wherein the metal ions are recovered from their salt forerunners over the interaction of plant metabolites; biomolecules that possess reduction capacities. The metal ions are transferred from their mono/divalent oxidation statuses to zero valent statuses, then nucleation of the reduced metal atoms occurs [23]. Then the growth phase comes wherein the separated metal atoms merge to form metal nanoparticles, however, additional biological reduction of metal ions happens. The growth phase increases in enhanced thermodynamic steadiness of nanoparticles while the widespread nucleation might cause aggregation of produced nanoparticles, changing their morphologies. The final phase in biosynthesis of nanoparticles is the stabilization phase. The nanoparticles eventually get their most intensely favorable and steady morphology when capped through plant metabolites. The effective mechanism of green synthesis using plants is shown in Fig. 2.

In fact, several characteristics of the solution combination such as; the concentration of metal salt, plant extract concentration, pH of the reaction solution, etc., and extra reaction circumstances such as reaction period and temperature have wide-ranging effects on the size, shape, and quality of the biosynthesized nanoparticles [24,25].

This study purposely focused on zinc oxide (ZnO) since ZnO is one of the most in-depth research semiconductor type metal oxides [26]. Among the semiconductor materials, ZnO possesses a wide band-gap of about 3.37 eV as well as an exciton binding energy of 60 meV [27] and Wurtzite structure (Fig. 3). Besides the semiconductor characteristic, ZnO possesses fascinating piezoelectric, [28] oxidizing, [29] antibacterial, and photo-catalytic characteristics [30]. Researchers utilize photo-catalytic characteristics by means of cannabinus fibers, nanohydrogel, nanocomposite hydrogel were used for effective adsorption of crystal violet dye, removing other dyes, and highly toxic metal ions from aqueous system [31–36]. Investigation of available studies on metallic and metal oxide NPs proposes that oxygen is normally an essential element for producing reactive oxygen species (ROS). Also, illumination is required for ROS production for metal oxide NPs [37–39].

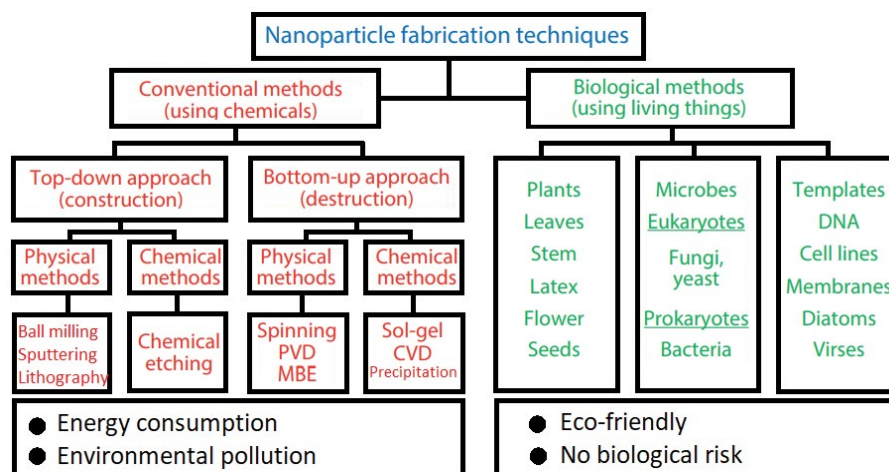


Fig. 1. Grouping of dissimilar nanoparticles production procedures.

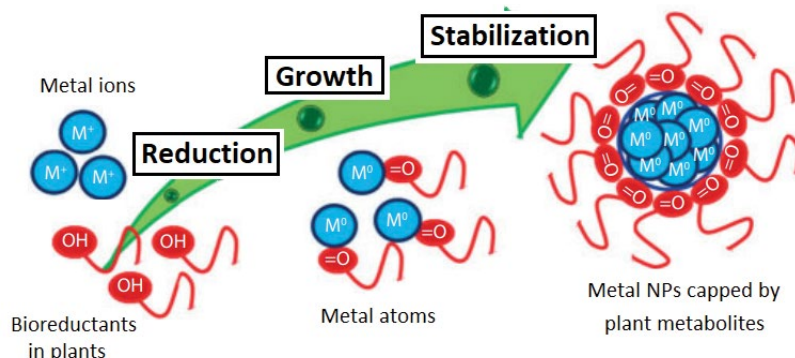


Fig. 2. Biosynthesis mechanism for producing metal NPs.

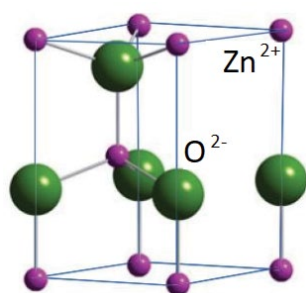


Fig. 3. Wurtzite structure of zinc oxide (ZnO).

As a photo-catalyst, ZnO and its nano-composites exhibit outstanding aptitude in the direction of the degradation of organic pollutants in water under the ultra-violet radiation [40]. Organic impurities experience degradation on the ZnO surface over the redox, that is, reduction and oxidation, procedures set by the electronic-excitation among valence and conduction bands. Similarly, ZnO possesses the capacity to produce reactive-oxygen species, namely ROS, under the ultra-violet radiation, which can degrade organic pollutants and deactivate or prevent microorganisms in water. Thus, as ZnO exhibits excellent photo-catalytic action, it could be utilized as an effective and feasible photo-catalyst for the degradation of organic pollutants in water. Nevertheless, the photo-catalytic action of ZnO is achieved when the particles are in the nano-size range (1–100 nm) contrary to the macroscopic or bulk size.

ZnO NPs showed a significant range of anti-coagulant activity [41–43] as well as numerous industrialized requests as a photo-catalyst for degradation of organic pollutants in addition to in solar energy adaptation equipment due to its effective photo activity, high steadiness, cheap price, and comparative harmlessness toward human beings and the surroundings [44]. Amongst ecological pollutants, azo dyes containing methyl orange (MO), in general, make up an important element of organic pollutants [45]. Azo dyes similar to methyl orange possess numerous undesirable concerns on ecological unit plagued by them [46]. Abundant research has been done on studying the decomposition of azo dyes utilizing  $TiO_2$  NPs and countless development has been made since the 1980s [47]. The significance of this study is ZnO NPs has been synthesized through an easy method that avoids toxic chemicals and difficult experimental processes.

Then the biosynthesized ZnO NPs from *Apium graveolens* L. leaf extract is utilized for photocatalytic activity, that is, removing the organic pollutants in water with interpretation the mechanism of degradation in detail.

## 2. Materials and methods

Zinc acetate dehydrate,  $Zn(CH_3COO)_2 \cdot 2H_2O$  Molecular weight 219.50 g/mol and purity >98.0%, sodium hydroxide pellets, NaOH Molecular weight 40 g/mol, and Methyl Orange (MO) ( $C_{14}H_{15}N_3O_3S$  Molecular weight 327.33 g/mol and purity >98.0%) were purchased from Sigma-Aldrich (Germany) and utilized as received-commercially with unpolluted specialized status. Fisher Scientific Company (USA) 11–600–49sh Isotemp Analog Hot Plate Stirrer was utilized as the heating source for the production of ZnO NPs. During the course of the ZnO NPs synthesis period, the hot plate was heated and the hot plate surface temperature was chosen to be around 80°C. UV-visible (UV-Vis) double beam was used for the photo-catalytic degradation of MO. X-ray diffraction (XRD) measurements were carried out using a PAN analytical (United Kingdom) X' Pert PRO ( $Cu K\alpha = 1.5406 \text{ \AA}$ ). The scanning rate was  $1 \text{ min}^{-1}$  in the  $2\theta$  range from 20° to 80°. UV-Vis spectral analysis was recorded on a double-beam spectrophotometer (Super Aquarius spectrophotometer) to ensure the formation of ZnO NPs. Morphology and particle dispersion was investigated by field emission scanning electron microscopy (FESEM) (Quanta 4500). The chemical composition of the prepared nanostructures was measured by EDX (energy-dispersive X-ray spectroscopy) performed in FESEM. FTIR analysis was carried out using a Perkin Elmer (USA). FTIR spectrophotometer with a resolution of  $4 \text{ cm}^{-1}$  was used for investigation of the functional groups in the leaf extract and the NPs. The shape and size of ZnO NPs were characterized by high-resolution transmission electron microscope (HRTEM) utilizing a Philips (USA) EM208 microscope functioning at an accelerating voltage of 90 kV. Differential scanning calorimetry (DSC) type (TA Instruments USA, DSC Q10) in the range 50°C–600°C was utilized for the DSC curve.

### 2.1. Preparation of plant extract

*A. graveolens* L. belongs to *Apiaceae* carrot family and its chemical composition contains choline ascorbate and

enzyme inositol triphosphate [48]. *Apium* was collected in Rashken (Latitude 36°11'58.0"N and Longitude 43°56'54.7"E) in Erbil city, Iraqi Kurdistan Region in spring season (April 2019). Fresh leaves of *A. graveolens* L. were washed several times with Distilled water, and then dehydrated to remove the remaining dust particles and moisture. Later, the leaves were converted to small pieces by cutting them. About 20 g of the small pieces of leaves and 5 mL of distilled water were put into a mortar and pestle and crushed into paste. Six grams of this paste was mixed with 100 mL of distilled water in a beaker, after that, 2 M of NaOH solution was added dropwise to regulate the pH of the mixture, observed by a pH meter, to pH 8. The pH was not selected arbitrarily, since according to the literatures, in general, smaller sized NPs produced at higher pH [49].

Then the mixture was stirred almost continuously for 1 h producing a cloudy precipitous of zinc hydroxide,  $Zn(OH)_2$ , which was then centrifuged at 5,000 rpm for 1 h and dried in an oven set to 60°C. After that the mixture cooled to room temperature (Fig. 4).

## 2.2. Synthesis of zinc oxide nanoparticles

ZnO NPs were prepared utilizing green synthesis method by means of *A. graveolens* L. extract. After preparation of the plant extract as described previously, 30 mL of this extract was put into a beaker and heated gradually. When the temperature reached 60°C, 3 g of zinc acetate were added to this extract. After that the mixture was continuously stirred, maintaining the temperature at 60°C, until the mixture converted into a yellowish paste after 1 h. It is obvious that, the temperature of reaction played important role in producing NPs, the optimal yield of NPs were achieved at 60°C. Afterward the paste was blazed in a furnace at 400°C for about 2 h then the residual was washed by ethanol and distilled water several times. The powder was then heated at 100°C to dry. Then zinc oxide nanoparticles

were obtained and they were ready for characterization. The middle of Fig. 4 shows the procedure of synthesizing zinc oxide nanoparticles using *A. graveolens* L. leaves extract and zinc acetate as a precursor.

## 2.3. Photocatalytic degradation of Methyl Orange

Photocatalytic degradation of Methyl Orange (MO) was first conducted in a Pyrex beaker with 150 mL volume. MO solutions possessing the concentration of 3 ppm (mg/L) were utilized for the photocatalytic tests. In the photo degradation experimentations, 25 mg of the biosynthesized ZnO NPs was evenly spread in 25 mL of MO solution using 3 min of bath sonication in dark-place. The bath sonication enabled the uniform spreading of the ZnO NPs along with assisting in the formation of the adsorption-desorption symmetry amongst the ZnO NPs as well as the dye. Then, 1 mL of the amalgamation sample was reserved and strained through a syringe-filter for UV-Vis spectroscopic investigation. The specific absorption maximum levels of MO located at 485 nm was utilized for calculating the degradation percentage. For the cyclical steadiness tests, the ZnO NPs were used in the first round was centrifuged and utilized in a similar way for the following sequences for the MO degradation. The sample was occupied from the centrifuged (4,000 rpm, 5 min) floating over with the intention of minimizing the loss of the ZnO NPs.

## 3. Results and discussion

### 3.1. Characterization of *Apium graveolens* L. leaf extract

Nowadays, in order to control the size and morphology of nanoparticles, investigators are using the individual plant phytochemicals for biosynthesizing nanoparticles. The phytochemicals presence in the plant extract reduces metal ion to metal nanoparticles. Therefore, plant extract, at the same time, acts as a reducing, and stabilizing agent.

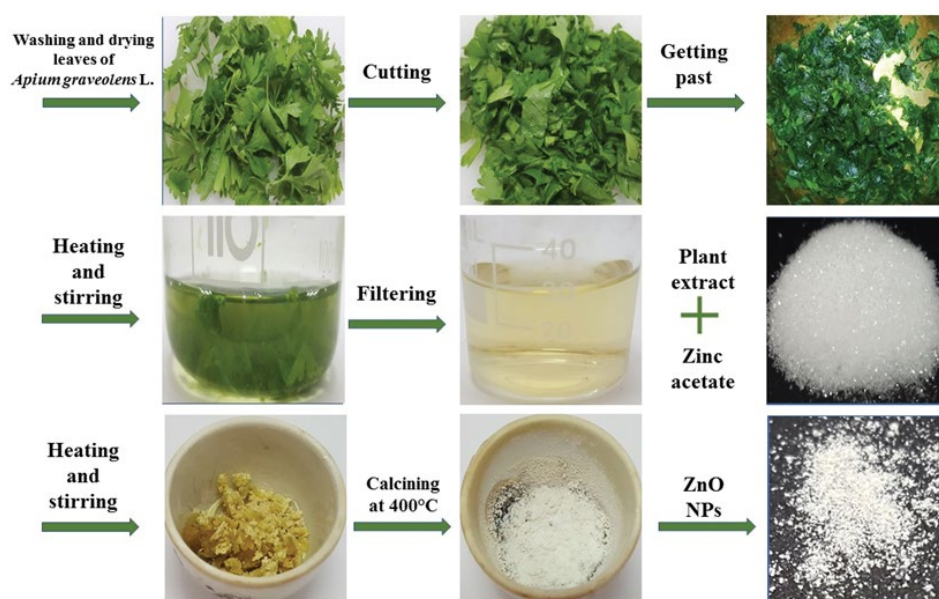


Fig. 4. Schematic representation of ZnO NPs synthesis using the leaf extract of *Apium graveolens* L. and zinc acetate dehydrate.

UV-Vis spectroscopy monitors this reaction progress. Spectra of UV-Vis spectroscopy displayed a peak absorption correlated with the surface plasmon resonance (SPR), and collects conduction band electrons oscillations in reacting with electromagnetic waves, representing metal ion reduction and nanoparticle formation. *A. graveolens* L. leaf extract contains flavonoid, polyphenols, carotenoid, lipid, polysaccharides, tannin, free organic acids, and essential oils (Fig. 5) which are considered as possible bio-reducing and stabilizing agents, due to the availability of OH groups, for nanoparticles synthesis [50,51]. These phytochemicals, being antioxidant and free from toxic chemicals, are extremely capable of reducing metal ions and stabilizing them in nanoscale dimension. They can also provide nanoparticles of different shapes and dimensions [52].

The OH groups form a complex of  $Zn(OH)_2$  with the zinc ions. The mechanisms of the phase transformation from  $Zn(OH)_2$  to ZnO takes place in three ways, that is, dissolution–reprecipitation, *in situ* crystallization and solid-solid phase transformation. The loss of water from the lattice throughout the solid–solid phase transformation has also been suggested by Wang et al. [53].

Fig. 6 shows the UV-Vis spectra of *A. graveolens* L. leaf extract. We deduced that the maximum peaks, at 264 and 325 nm, might be associated with phenolic components and flavonoid existing in *A. graveolens* L. leaf extract. The functional organic-molecules such as Apiin, phenol, ascorbic acid exists in the *A. graveolens* L. leaf extract [54]. Liu et al. [55] stated that these peaks related to Apiin,  $C_{26}H_{28}O_{14}$  a natural flavonoid found in *A. graveolens* L. leaf extract. Makarov et al. [56] claims that flavonoids, in general, through their OH group switched from the enol-form to the keto-form [57], donating a responsive hydrogen atom which reduces the metallic ion into nanoparticles. Among those functional organic-molecules the phenolic combinations existing in the extract more likely had great empathies on the metals [58], that reduced  $Zn^{2+}$  to  $Zn^0$  [59]. Throughout air-drying, the produced  $Zn^0$  were oxidized to produce ZnO NPs [60].

The Fourier transform infrared (FTIR), spectra of the plant extract and ZnO NPs were examined to figure out if the functional groups related to these reductive biomolecules exists and specifying the functional groups that contributed to reduction of the ZnO into nanoparticles. The FTIR spectrum of *A. graveolens* L. leaf extract (Fig. 7) contains numerous clear peaks through the whole range. In general, an FTIR spectra has two regions, that is, the functional group region ( $1,800\text{--}4,000\text{ cm}^{-1}$ ) as well as the fingerprint region ( $0\text{--}1,500\text{ cm}^{-1}$ ). The bands at  $1,645$  and  $3,383\text{ cm}^{-1}$  point toward C=O stretching of tertiary-amides and O–H stretching of phenol group, correspondingly [61]. A band at  $1,079\text{ cm}^{-1}$  pointed toward the C–N stretching vibration of amines while a separate band at  $1,562\text{ cm}^{-1}$  indicates the bending of C–H bonds existing in hydrocarbons [62] that stick to the surface during ZnO NPs synthesis. The bands detected at  $1,422$  and  $667\text{ cm}^{-1}$  could be associated to C–H bending of alkanes and stretching vibrations of halo-alkanes in that order [63].

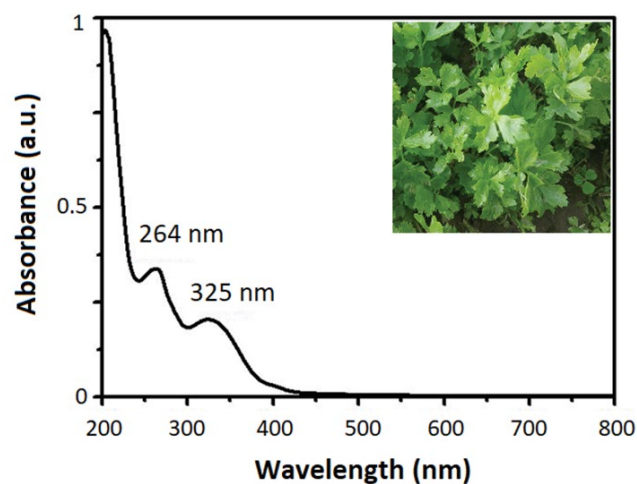


Fig. 6. UV-Vis spectra of *Apium graveolens* L. leaf extract.

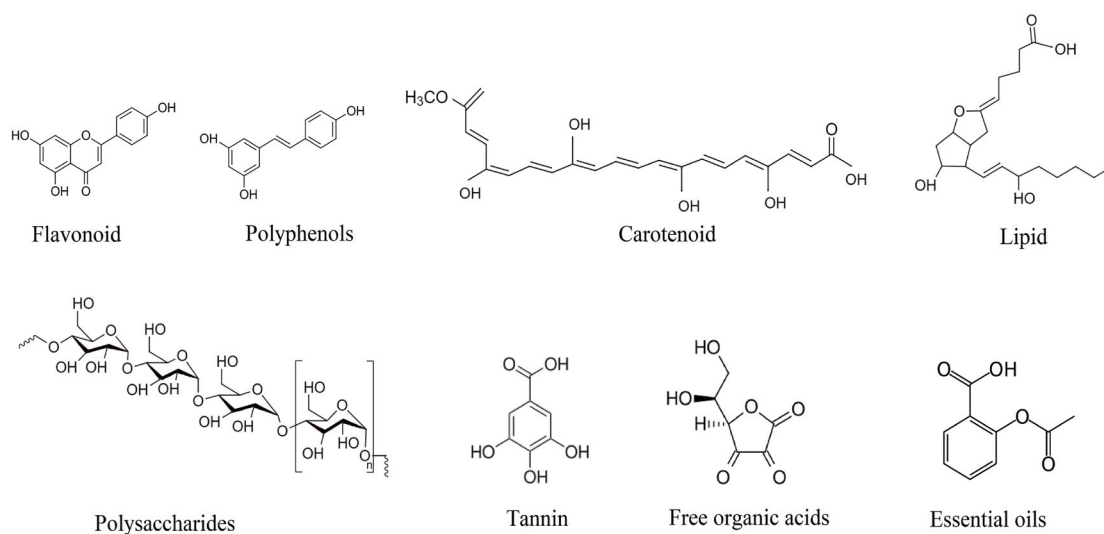


Fig. 5. Available phytochemicals in *Apium graveolens* L. leaf extract.

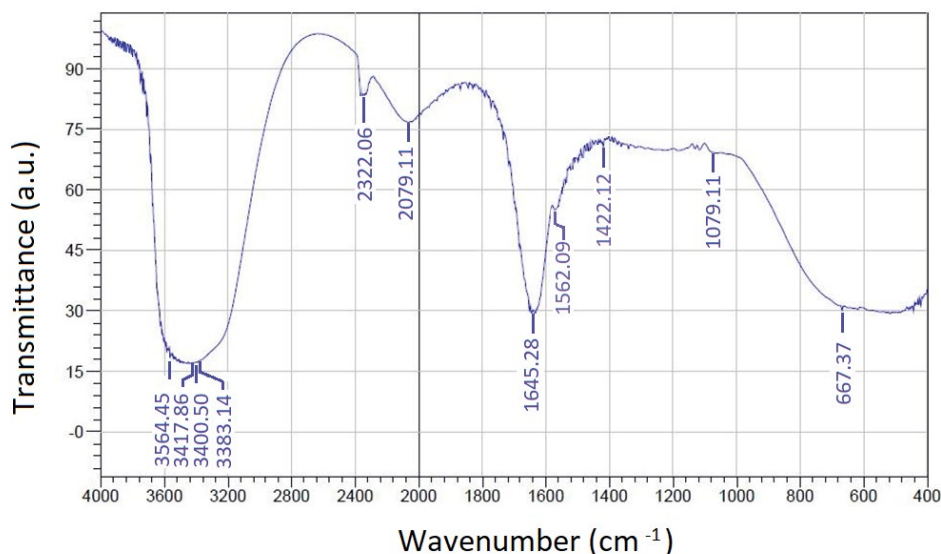


Fig. 7. FTIR spectra of *Apium graveolens* L. leaf extract.

### 3.2. Characterization of ZnO NPs

In this study, numerous techniques were utilized to describe the structure, morphology, optical, thermal, and photocatalytic properties of ZnO NPs.

#### 3.2.1. UV-Vis analysis

UV-Vis spectroscopy (Fig. 8) revealed a peak at 370 nm, which was typical of ZnO NPs. This was owing to the SPR, and the sharpened peak confirmed the construction of mono-dispersed ZnO NPs [64]. As a rule of thumb, the absorption peak maximum for ZnO NPs ranges between 300 and 380 nm [65]. The assessed value is lower than that of bulk ZnO given as 380 nm [66] and display a blue shift in excitonic-absorption which specifies a tiny quantum confinement consequence [67].

The straightforward band-gap energy ( $E_g$ ) for the ZnO NPs is characterized through fitting the reflection data to the straight transform formula  $\alpha hv = A(hv - E_g)^n$ , where  $\alpha$  is the optical-absorption parameter,  $hv$  is the energy of photon,  $E_g$  is the straight band-gap,  $A$  is a constant, and the power  $n$  is influenced by the type of optical-transition that predominates. Precisely, with  $n = 1/2$ , an optimum straightness has been perceived for the straight permitted transition, the best choice in the method considered here. The specific amount of the band-gap is described through the extrapolation of the rectilinear part of  $(\alpha hv)^2$  vs.  $hv$  to the  $x$ -axis. The straight band-gap is equals to 3.132 eV for ZnO NPs which is shown in Fig. 8. A decrease in the band-gap is expected as a result of using plant extract, since some plant extract component covers/modifies the surface and reduce the band-gap of the nanoparticles [68]. This consequence does not conflict with the quantum confinement effects especially for the green synthesized nanoparticles. In general, the biosynthesized nanoparticles are more reactive than the equivalent nanoparticles prepared from the other methods [69]. Therefore, the overall high reactivity of particles in the quantum regime can also be attributed to increase in electron populations at the

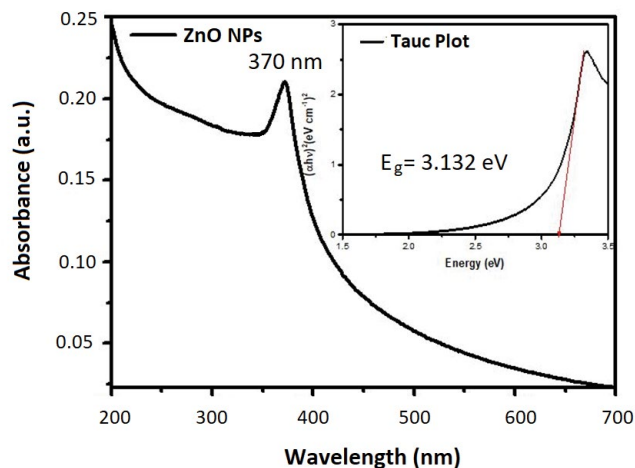


Fig. 8. UV-Vis spectrum of ZnO nanoparticles prepared by *Apium graveolens* L. leaf extract and zinc acetate dehydrate, inset: Tauc plot of the same UV-Vis spectrum.

lower energy bands, due to decreased separation of energy states [70]. Metal NPs possess sizes which are much smaller than the wavelength of visible light. They make interaction with light and they can absorb or scatter light. Metal oxides in their bulk status possess a wide band-gap and fewer ability to interact [71] but once their dimensions are decreased, they become supplementary responsive and their aptitude to interact can be inferred from their reflectivity and absorbance capabilities. The absorption peak for ~40 nm ZnO NPs has been described by Singh et al. [72] at 361 nm (3.44 eV) and 3.44 eV for the chemical synthesis of ZnO NPs [73], respectively.

#### 3.2.2. FTIR spectroscopy analysis

The FTIR spectrum (Fig. 9), utilized to inspect the pureness and composition of biosynthesized ZnO NPs, reveals

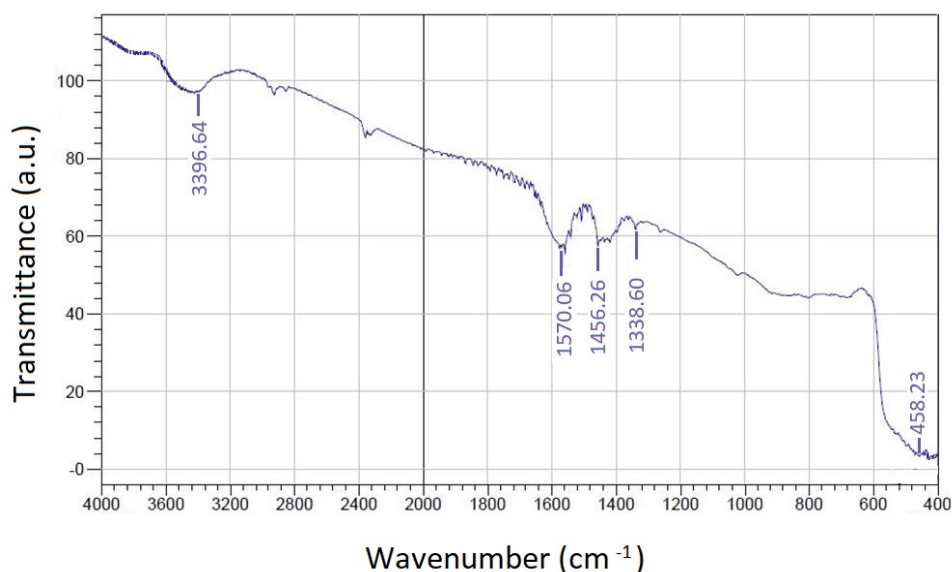


Fig. 9. FTIR spectra of biosynthesized ZnO nanoparticles.

no distinct peak in the monitoring range intimating pureness of the ZnO nanoparticles produced by the green process. The broad band at  $667\text{ cm}^{-1}$  vanished in the synthesized ZnO nanoparticles. Another peak was formed at  $458\text{ cm}^{-1}$  as a result of the formation of ZnO nanoparticles, precisely zinc and oxygen bonding vibrations [74,75]. The band at  $1,338\text{ cm}^{-1}$  correlated to the C–O stretching of the carboxylic acid group. Numerous bands found between  $1,400$  and  $1,600\text{ cm}^{-1}$  related to the –C=C– stretching of the aromatic compounds [76]. The robust and relatively wide band at  $3,396\text{ cm}^{-1}$  could be allocated to the O–H stretching of phenolic compounds [77].

### 3.2.3. XRD analysis

XRD analysis (Fig. 10) revealed the  $2\theta$  characteristic peaks of ZnO at  $31.60^\circ$ ,  $34.22^\circ$ ,  $36.11^\circ$ ,  $47.35^\circ$ ,  $56.45^\circ$ ,  $62.69^\circ$ ,  $66.11^\circ$ ,  $67.84^\circ$ ,  $68.87^\circ$ ,  $71.70^\circ$ , and  $76.64^\circ$  for (100), (002), (101), (102), (110), (103), (200), (112), (201), (004), and (202) planes of the crystal lattice, correspondingly. These peaks were agreeable with the regular JCPDS card No. 89–0510 and proposed the existence of hexagonal Wurtzite form of ZnO NPs. The narrow and robust diffraction peaks point toward the optimum crystalline structure of ZnO NPs. The average crystallite sizes of ZnO NPs were calculated using Debye–Scherrer’s equation, that is,  $D = k\lambda/\beta\cos\theta$ , where  $D$  is crystal size,  $\lambda$  is the wavelength of the X-ray radiation ( $\lambda = 0.15406\text{ nm}$ ) for Cu  $K_\alpha$ ,  $k$  is shape factor typically taken as 0.89,  $\beta$  is the full width at high maximum (FWHM), and  $\theta$  is the diffraction angle [78].

According to Debye–Scherrer’s equation the average crystallite size for ZnO NPs was  $28\text{ nm}$  confirmed the nano-size of the ZnO NPs (Table 1). Similar outcomes were found for the biosynthesized ZnO NPs utilizing *Peltophorum pterocarpum* leaf extract [64], *Adhatoda vasica* leaf extract [79], and *Arabic gum* [80].

XRD analysis confirmed the existence of even tinier nanoparticles than the SEM inspection. The larger ZnO

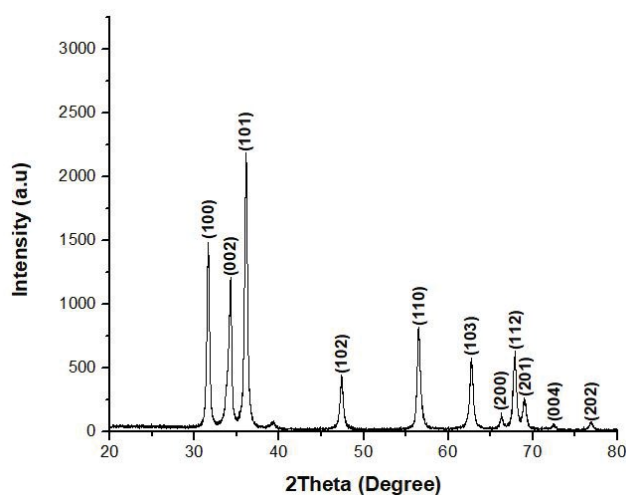


Fig. 10. XRD patterns of ZnO NPs prepared by the biosynthesis method.

nanoparticles in the sample caused by the agglomeration of smaller nanoparticles, whose existence is indicated by XRD. The XRD method allowed for the identifying smaller dimensions of nanoparticles.

### 3.2.4. SEM analysis

The surface morphology of the biosynthesized ZnO NPs was principally characterized using FESEM analysis and the resulting images are displayed in Fig. 11. It can be noticed that most of the ZnO NPs are in nanometer scale and are vastly semi-spherical particles with the average diameter of  $35\text{ nm}$ . Remarkably, the greatest amount of the ZnO NPs are identical in dimension together with an insufficient large particles (Fig. 11). In addition, the ZnO NPs are slightly agglomerated which is typical with the green synthesis

Table 1  
The ZnO NPs particle size calculation using Debye-Scherrer's equation and data from Fig. 8

No. of peaks	Planes	Pos. [ $^{\circ}2 \text{ Th.}$ ]	FWHM [ $^{\circ}2 \text{ Th.}$ ]	Size (nm)
1	100	31.6341	0.2755	29.97068
2	002	34.2867	0.2558	32.50064
3	101	36.0837	0.2362	35.37301
4	102	47.4023	0.3542	24.49485
5	110	56.46	0.3149	28.63379
6	103	62.753	0.3542	26.27051
7	200	66.2729	0.3149	30.12759
8	112	67.8717	0.2362	40.53903
9	201	69.1166	0.3936	24.50814
10	004	72.3986	0.9446	10.422
11	202	76.8586	0.3936	25.76498
Average size				28.05502

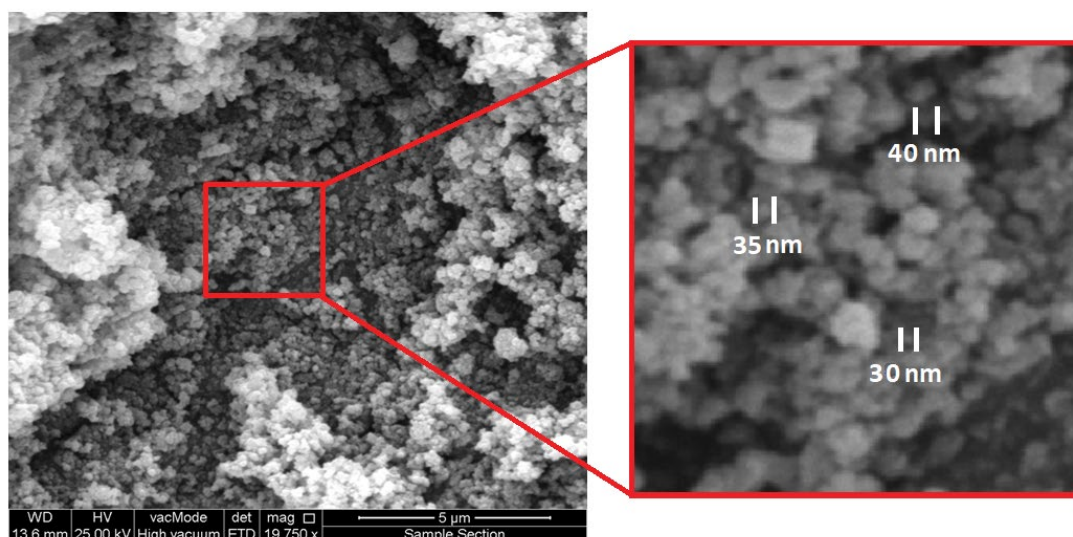


Fig. 11. FESEM of ZnO NPs synthesized from *Apium graveolens* L. leaf extract.

nanoparticles. This is due to the fact that biosynthesis NPs possess higher surface area and the durable affinity amongst them cause aggregation or agglomeration [81]. It can be stated that, the ecological factors highly influence the stability of NPs and agglomeration. Thus, throughout the process of nanoparticles formation the NPs stick to each other and impulsively form asymmetrical clusters [82].

Production procedure of ZnO NPs relies upon several growth parameters, comprising concentration of plant extract or biomass, concentration of salt, growth or reaction time, temperature, and pH of the solution. Therefore, calibration of these growth elements is essential in gaining the required size and shape of NPs for their maximum manipulation and request.

### 3.2.5. EDX analysis

In order to expand supplementary vision into the topographies of ZnO NPs, the exploration of the sample was

investigated by means of EDX analysis. The EDX spectra of the samples taken from the SEM investigation displaying that the sample produced through the above method has clean ZnO phase [83]. The EDX analysis (Fig. 12) of the ZnO NPs indicates that our sample contains zinc, oxygen, and gold as essential elements. The EDX spectra displayed two robust peaks for zinc around 1 and 8.7 keV, correspondingly and a singular peak for oxygen at  $\sim 0.5$  keV, which are typical for ZnO NPs [84]. The presence of gold is as a result of the sample coating throughout FESEM imaging. The high-intensity of zinc and oxygen peaks show that the sample is mostly ZnO.

### 3.2.6. HRTEM analysis

Fig. 13a shows the HRTEM image of the ZnO nanoparticles. It can be seen that, the ZnO NPs possess a semi-spherical morphology as confirmed by FESEM previously with almost a uniform size. The magnification in Fig. 13a shows single ZnO particles with a diameter between 30 and 40 nm.

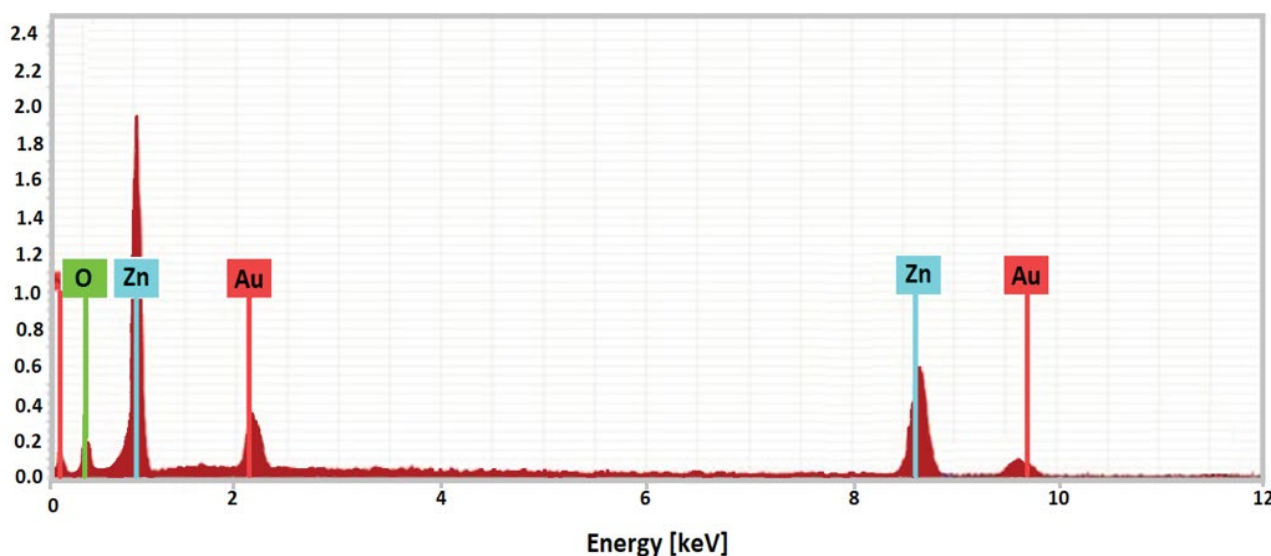


Fig. 12. EDX profile of ZnO NPs biosynthesized from *Apium graveolens* L. leaf extract.

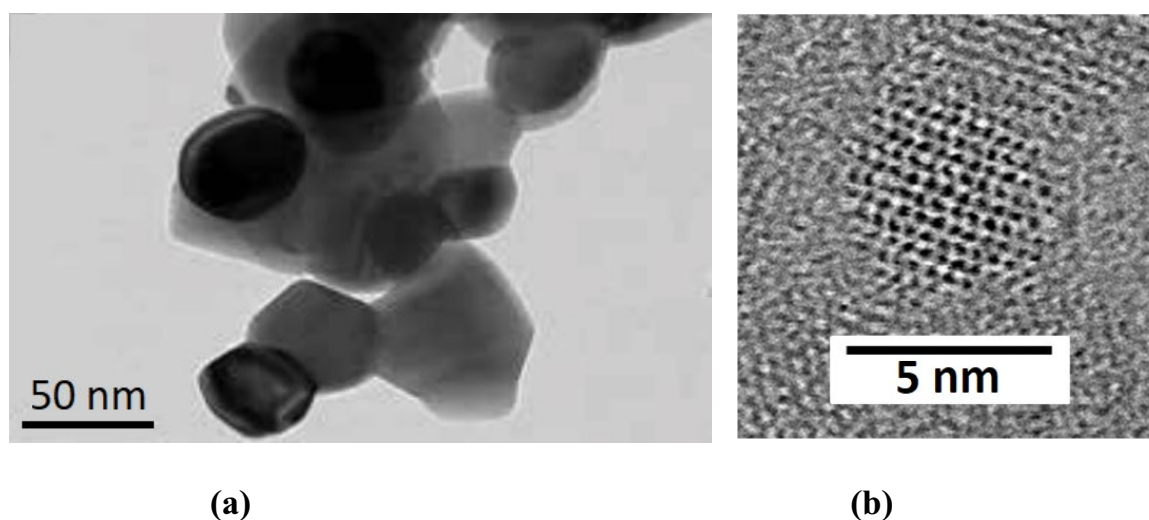


Fig. 13. (a) HRTEM image of ZnO NPs from biosynthesis method and (b) high-resolution of a plane of the Wurtzite type structure.

This magnification, Fig. 13b, also displays that the particle is crystalline, as the lattice planes are recognizable and it has hexagonal Wurtzite shape. There are no lattice defects, such as dislocations, which confirm the high crystallinity as indicated by XRD pattern before.

### 3.2.7. DSC analysis

DSC can validate an alteration in melting temperatures depending on grain size. Generally, the melting temperature of nanoparticles can be  $-263.15$  to  $-173.15^\circ\text{C}$  beneath the bulk material due to a greater value of surface/volume ratio [85]. DSC analysis was utilized to describe the decomposition and thermal stability of nanoparticles measured from  $50^\circ\text{C}$  to  $600^\circ\text{C}$  at the heating rate of  $10^\circ\text{C}/\text{min}$ . It can be seen, from Fig. 14, that the DSC curve of the biosynthesized

ZnO NPs exhibits two endothermic peaks with one exothermic peak centered at about  $111.35^\circ\text{C}$ ,  $223^\circ\text{C}$ ,  $271.95^\circ\text{C}$ , and  $365.11^\circ\text{C}$ , respectively. A tiny endothermic peak recorded near  $111.35^\circ\text{C}$ , initiated at  $100^\circ\text{C}$  is assigned to the vaporization of the absorbed water by ZnO NPs. This tiny displacement from  $100^\circ\text{C}$  to  $111.35^\circ\text{C}$  might be ascribed to the loss of unstable wetting agent molecules adsorbed on the surface of ZnO NPs throughout synthesizing process [86]. While, the exothermic peak that appeared at  $365.11^\circ\text{C}$  is, perhaps, owing to the formation of ZnO NPs and degradation of organic materials. This is a good indicator that, despite the crystallinity of the ZnO NPs which has been verified by XRD analysis (Fig. 10), the ZnO NPs need further annealing until around  $365^\circ\text{C}$  in order to be more purified. Lastly, the peak nearby  $271.95^\circ\text{C}$  is, most likely, allocated to the alteration of zinc complex to zinc hydroxide ( $\text{Zn}(\text{OH})_2$ ) [87].

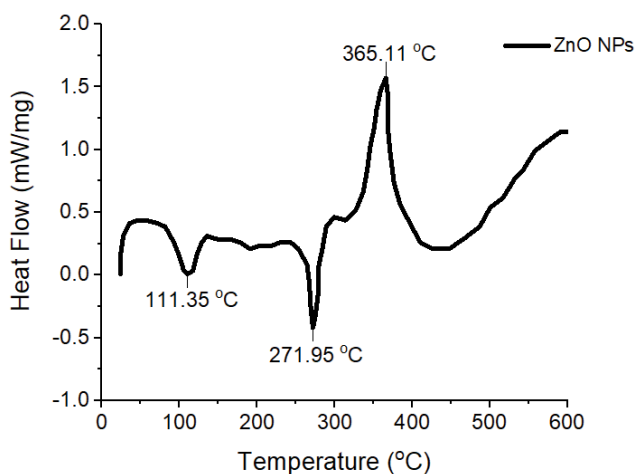


Fig. 14. Differential scanning calorimetry curve of the biosynthesized ZnO NPs.

### 3.3. Degradation of Methyl Orange

The mechanism of photocatalysis reactions has been massively studied by several authors [88–91]. In the beginning, UV-Vis radiation interacts with the nanoparticles, causing the formation of an electron-hole pair. This pair migrates to the semiconductor surface and may recombine at any time. When the pair reaches the surface, the electron is transferred to an acceptor molecule, while an electron of a donor molecule is transferred to the gap. Since electron-gap recombination occurs in microseconds, there is a need for a smaller semiconductor particle size, nanoparticles, so that more migrations and reactions occur before recombination of the electron-gap pair, optimizing the production of radicals  $\text{OH}^*$  relative to the number of absorbed photons [92].

In general, electron donor and receptor molecules determine which photochemical process will occur. Fig. 15 shows a scheme that clarifies the photocatalysis mechanism. The following equations explain the possible photocatalysis

mechanism of pollutant degradation by the radical  $\text{OH}^*$ . After the generation of the electron-gap pair ( $e_{\text{c.b.}}^- + h_{\text{v.b.}}^+$ ) through the energy absorption ( $h\nu$ ) in the ZnO NPs, a water molecule interacts with the gap ( $h_{\text{v.b.}}^+$ ) and undergoes the oxidation state to generate the radical  $\text{OH}^*$ . Similarly, an oxygen molecule interacts with the electron ( $e_{\text{c.b.}}^-$ ) and is reduced to the formation of the radical  $\text{O}_2^{\bullet -}$ . This radical  $\text{O}_2^{\bullet -}$  can be reduced by attacking water to form  $\text{H}_2\text{O}_2$ , which is more reduced to form a radical  $\text{OH}^*$  and an  $\text{OH}^-$  ion. Moreover, this ion may be oxidized to form another radical  $\text{OH}^*$ . Explicitly, the radicals  $\text{OH}^*$  and  $\text{O}_2^{\bullet -}$  are responsible for the degradation of the pollutant under UV-light radiation.



It can be stated that, methyl orange is classified among illustrative AZO type of dyes, which are particularly significant type of artificial organic-dyes utilized in the textiles sector and are similarly regular manufacturing contaminants [93]. The photocatalytic degradation degree was investigated through the absorbance lowering of the solution. Fig. 16 displays a characteristic UV-Vis spectrum of the methyl orange degradation as a function of time.

The absorption peaks consistent with methyl orange dye vanished after 3 min photo-irradiation. The swift vanishing of the absorption peaks in Fig. 16 proposes that the

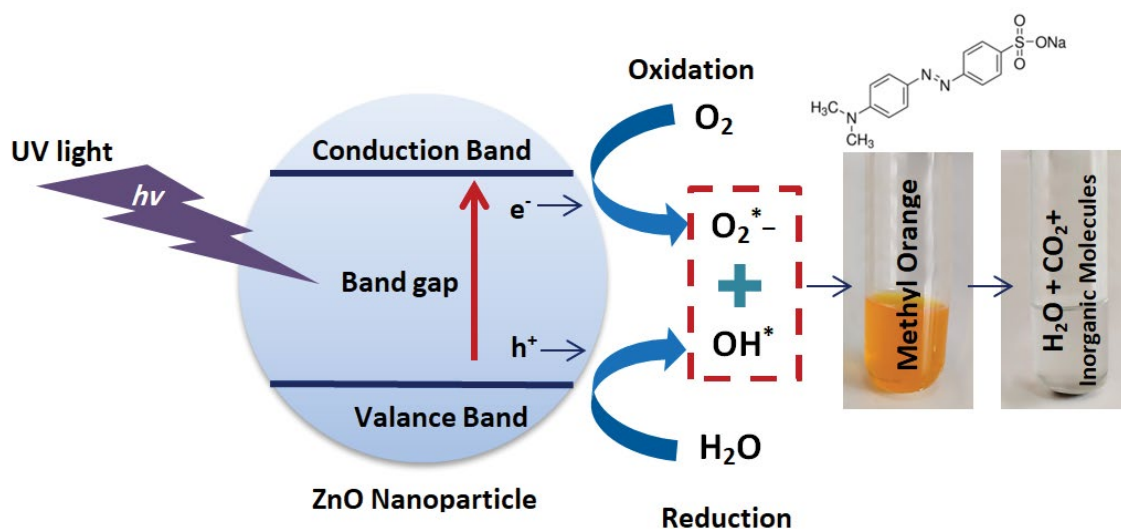


Fig. 15. Mechanism for degradation of methyl orange using biosynthesized NPs.

functional-group are liable for the typical color of the methyl orange dye. Even with very low UV power, the biosynthesized ZnO NPs can degrade existing methyl orange in water effectively. This is due to the fact that the photocatalytic action of ZnO NPs strongly relies upon the growing orientation of the crystal plane. For instance, the radical  $\text{OH}^{\bullet}$ , a non-selective, and influential oxidant is intended to attack one of the aromatic-rings of the methyl orange ( $\text{C}_{14}\text{H}_{14}\text{N}_3\text{NaO}_3\text{S}$ ) and causes the degradation. The radicals adsorbing on catalytic surface or existing freely in the solution can lead to the photo degradation of methyl orange dye which is adsorbed on the catalytic surface or existent freely in the solution [94]. Indeed,

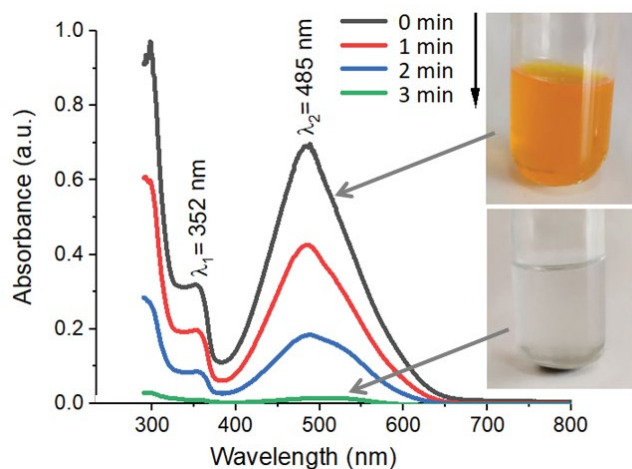


Fig. 16. Time-dependent UV-Vis absorption measurement of methyl orange degradation using ZnO NPs.

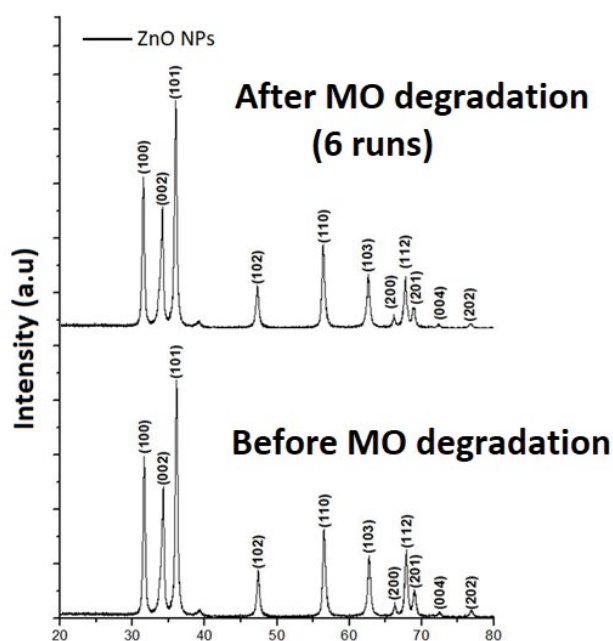


Fig. 17. XRD patterns before and after degradation of MO in water using ZnO NPs for six runs.

the nature of by-products designed relies on the diverse replacement locations of  $\text{OH}^{\bullet}$  in methyl orange fraction. Degradation path are connected mainly with hydroxylation and demethylation procedures causing the creation of unbalanced semi-processes which can effortlessly experience ring opening procedure [95].

Fig. 17 shows the reusability of ZnO NPs for the degradation of MO over six cycles. After photocatalytic investigation, the catalyst was segregated from the reaction mixture through centrifugation and washed with distilled water and ethanol till a clear supernatant was acquired. The washed catalyst was dried at  $80^{\circ}\text{C}$  for 1 h and reused again for the degradation of a newly prepared MO dye solution where the concentration of the dye solution was fixed to its original value. Besides, the XRD pattern was recorded to compare crystalline structures of ZnO NPs before and after recycling process. According to Fig. 17, the crystalline phase and structure of the ZnO NPs after six cycles precisely overlapped with those of the sample before the reaction. This can give sensible clarification to the fact why the ZnO NPs photocatalyst display a very good photostability. Our results indicate that the ZnO NPs from *A. graveolens* L. leaf extract exhibited high photo-catalytic activity, explicitly can cleanse the water from methyl orange dye in a very short time and the ZnO NPs are reusable for several times.

#### 4. Conclusions

Biosynthesis of ZnO NPs with the use of plant extract has improved remarkably due to their heterogeneous requests. This study involved, a quick and economic biosynthesis of ZnO NPs from zinc acetate using aqueous leaf extract of *A. graveolens* L. and their catalytic degradation of methyl orange (MO) dye. The effective ingredients existent in *A. graveolens* L. leaf extract are behaving as a reducing agent along with the capping and stabilizing agents for the production of ZnO nanoparticles.

Several techniques, namely UV-Vis spectroscopy, FTIR analysis, XRD, SEM, TEM, EDX, and DSC have been utilized in this investigation to analyze both the property and quality of the biosynthesized ZnO NPs. These techniques showed that the property of the biosynthesized ZnO NPs is comparable with the standard NPs prepared from different methods.

Removing the organic pollutants in water was our target application of biosynthesized ZnO NPs. The charge transfer procedure among methyl orange molecules and ZnO NPs was investigated utilizing UV-Vis spectrometer. The ZnO NPs can directly decompose methyl orange dye deprived of the support of radicals. Methyl orange can be degraded by electrons and holes in ZnO NPs. In waste water treatment by ZnO NPs, the competition between the holes of ZnO and the  $\text{OH}^{\bullet}$  radicals towards decomposing methyl orange relies upon the concentration of methyl orange. The consequences of this study indicated that the biosynthesized ZnO NPs displayed high photocatalytic activity, that is, can purify the water in a very short time and reproducible for several times. Thus, ZnO NPs prepared by the green method could be the best candidate for water purification, through photo-catalysis, in addition to other ecological requests.

## Acknowledgments

Himdad Hamad Azeez is thankful to Salahaddin University-Erbil, Iraq, for being an MSc. student and fully supported by them. The authors would like to thank Soran research center for providing all the facilities to perform the research work. In addition, the authors thank Dr. Mukhtar Ahmed at SISAF, Ulster University, UK, Garmian University, and Koya University for their valuable assistance throughout this investigation. Finally, a sincere thank goes to Dr. David M.W. Waswa at Tishk International University for his diligent proofreading of this manuscript.

## References

- [1] P. Boisseau, B. Loubaton, Nanomedicine, nanotechnology in medicine, *C. R. Phys.*, 12 (2011) 620–636.
- [2] S.S. Suri, H. Fenniri, B. Singh, Nanotechnology-based drug delivery systems, *J. Occup. Med. Toxicol.*, 2 (2007) 16.
- [3] S. Bhattacharya, I. Saha, A. Mukhopadhyay, D. Chattopadhyay, U. Chand, Role of nanotechnology in water treatment and purification: potential applications and implications, *Int. J. Chem. Sci. Technol.*, 3 (2013) 59–64.
- [4] M. Rai, A. Ingle, Role of nanotechnology in agriculture with special reference to management of insect pests, *Appl. Microbiol. Biotechnol.*, 94 (2012) 287–293.
- [5] T.V. Duncan, Applications of nanotechnology in food packaging and food safety: barrier materials, antimicrobials and sensors, *J. Colloid Interface Sci.*, 363 (2011) 1–24.
- [6] T. Stelzner, M. Pietsch, G. Andrä, F. Falk, E. Ose, S. Christiansen, Silicon nanowire-based solar cells, *Nanotechnology*, 19 (2008) 295203.
- [7] S. Raj, S. Jose, U. Sumod, M. Sabitha, Nanotechnology in cosmetics: opportunities and challenges, *J. Pharm. Bioallied. Sci.*, 4 (2012) 186–193.
- [8] Y. Wong, C. Yuen, M. Leung, S. Ku, H. Lam, Selected applications of nanotechnology in textiles, *Autex Res. J.*, 6 (2006) 1–8.
- [9] S. De Franceschi, L. Kouwenhoven, Nanotechnology: electronics and the single atom, *Nature*, 417 (2002) 701.
- [10] H.-L. Liu, S.A. Dai, K.-Y. Fu, S.-h. Hsu, Antibacterial properties of silver nanoparticles in three different sizes and their nanocomposites with a new waterborne polyurethane, *Int. J. Nanomed.*, 5 (2010) 1017–1028.
- [11] Y.A. Krutyakov, A.A. Kudrinskiy, A.Y. Olenin, G.V. Lisichkin, Synthesis and properties of silver nanoparticles: advances and prospects, *Russ. Chem. Rev.*, 77 (2008) 233–257.
- [12] R. Geethalakshmi, D. Sarada, Characterization and antimicrobial activity of gold and silver nanoparticles synthesized using saponin isolated from *Trianthema decandra* L., *Ind. Crop Prod.*, 51 (2013) 107–115.
- [13] I. Aiad, M.M. El-Sukkary, E. Soliman, M.Y. El-Awady, S.M. Shaban, In situ and green synthesis of silver nanoparticles and their biological activity, *J. Ind. Eng. Chem.*, 20 (2014) 3430–3439.
- [14] M.M. Stevanović, S.D. Škapin, I. Bračko, M. Milenković, J. Petković, M. Filipić, D.P. Uskoković, Poly (lactide-co-glycolide)/silver nanoparticles: synthesis, characterization, antimicrobial activity, cytotoxicity assessment and ROS-inducing potential, *Polymer*, 53 (2012) 2818–2828.
- [15] R. Wahab, A. Mishra, S.-I. Yun, Y.-S. Kim, H.-S. Shin, Antibacterial activity of ZnO nanoparticles prepared via non-hydrolytic solution route, *Appl. Microbiol. Biotechnol.*, 87 (2010) 1917–1925.
- [16] M. Premanathan, K. Karthikeyan, K. Jeyasubramanian, G. Manivannan, Selective toxicity of ZnO nanoparticles toward Gram-positive bacteria and cancer cells by apoptosis through lipid peroxidation, *Nanomedicine*, 7 (2011) 184–192.
- [17] Y.S. Lee, D.W. Kim, Y.H. Lee, J.H. Oh, S. Yoon, M.S. Choi, S.K. Lee, J.W. Kim, K. Lee, C.-W. Song, Silver nanoparticles induce apoptosis and G2/M arrest via PKC $\zeta$ -dependent signaling in A549 lung cells, *Arch. Toxicol.*, 85 (2011) 1529–1540.
- [18] M. Arabi, M. Ghaedi, A. Ostovan, Development of a lower toxic approach based on green synthesis of water-compatible molecularly imprinted nanoparticles for the extraction of hydrochlorothiazide from human urine, *ACS Sustainable Chem. Eng.*, 5 (2017) 3775–3785.
- [19] J. Liu, S.Z. Qiao, Q.H. Hu, G.Q. Lu, Magnetic nanocomposites with mesoporous structures: synthesis and applications, *Small*, 7 (2011) 425–443.
- [20] P. Mohanpuria, N.K. Rana, S.K. Yadav, Biosynthesis of nanoparticles: technological concepts and future applications, *J. Nanopart. Res.*, 10 (2008) 507–517.
- [21] A.T. Marshall, R.G. Haverkamp, C.E. Davies, J.G. Parsons, J.L. Gardea-Torresdey, D. van Agterveld, Accumulation of gold nanoparticles in *Brassic juncea*, *Int. J. Phytorem.*, 9 (2007) 197–206.
- [22] J. Kim, Y. Rheem, B. Yoo, Y. Chong, K.N. Bozhilov, D. Kim, M.J. Sadowsky, H.-G. Hur, N.V. Myung, Peptide-mediated shape- and size-tunable synthesis of gold nanostructures, *Acta Biomater.*, 6 (2010) 2681–2689.
- [23] P. Malik, R. Shankar, V. Malik, N. Sharma, T.K. Mukherjee, Green chemistry based benign routes for nanoparticle synthesis, *J. Nanopart.*, 2014 (2014) 302429–302443.
- [24] A.D. Dwivedi, K. Gopal, Biosynthesis of silver and gold nanoparticles using *Chenopodium album* leaf extract, *Colloid Surf., A*, 369 (2010) 27–33.
- [25] A.K. Mittal, Y. Chisti, U.C. Banerjee, Synthesis of metallic nanoparticles using plant extracts, *Biotechnol. Adv.*, 31 (2013) 346–356.
- [26] A.B. Djurišić, Y.H. Leung, A.M.C. Ng, Strategies for improving the efficiency of semiconductor metal oxide photocatalysis, *Mater. Horiz.*, 1 (2014) 400–410.
- [27] A. Król, P. Pomastowski, K. Rafińska, V. Railean-Plugaru, B. Buszewski, Zinc oxide nanoparticles: synthesis, antiseptic activity and toxicity mechanism, *Adv. Colloid Interfaces*, 249 (2017) 37–52.
- [28] Z.L. Wang, J. Song, Piezoelectric nanogenerators based on zinc oxide nanowire arrays, *Science*, 312 (2006) 242–246.
- [29] T. Xia, M. Kovoichich, M. Liong, L. Madler, B. Gilbert, H. Shi, J.I. Yeh, J.I. Zink, A.E. Nel, Comparison of the mechanism of toxicity of zinc oxide and cerium oxide nanoparticles based on dissolution and oxidative stress properties, *ACS Nano*, 2 (2008) 2121–2134.
- [30] K. Qi, B. Cheng, J. Yu, W. Ho, Review on the improvement of the photocatalytic and antibacterial activities of ZnO, *J. Alloy Compd.*, 727 (2017) 792–820.
- [31] G. Sharma, M. Naushad, D. Pathania, A. Mittal, G. El-Desoky, Modification of *Hibiscus cannabinus* fiber by graft copolymerization: application for dye removal, *Desal. Water Treat.*, 54 (2015) 3114–3121.
- [32] G. Sharma, M. Naushad, H. Aláa, A. Kumar, M.R. Khan, S. Kalia, M. Bala, A. Sharma, Fabrication and characterization of chitosan-crosslinked-poly (alginate acid) nanohydrogel for adsorptive removal of Cr(VI) metal ion from aqueous medium, *Int. J. Biol. Macromol.*, 95 (2017) 484–493.
- [33] M. Naushad, G. Sharma, Z.A. Allothman, Photodegradation of toxic dye using Gum Arabic-crosslinked-poly (acrylamide)/Ni(OH) $_2$ /FeOOH nanocomposites hydrogel, *J. Cleaner Prod.*, 241 (2019) 118263.
- [34] G. Sharma, A. Kumar, M. Naushad, A. García-Peñas, H. Aláa, A.A. Ghfar, V. Sharma, T. Ahamad, F.J. Stadler, Fabrication and characterization of Gum arabic-cl-poly (acrylamide) nanohydrogel for effective adsorption of crystal violet dye, *Carbohydr. Polym.*, 202 (2018) 444–453.
- [35] G. Sharma, D. Pathania, M. Naushad, N. Kothiyal, Fabrication, characterization and antimicrobial activity of polyaniline Th(IV) tungstomolybdo phosphate nanocomposite material: efficient removal of toxic metal ions from water, *Chem. Eng. J.*, 251 (2014) 413–421.
- [36] M. Naushad, S. Vasudevan, G. Sharma, A. Kumar, Z. AlOthman, Adsorption kinetics, isotherms, and thermodynamic studies for Hg $^{2+}$  adsorption from aqueous medium using alizarin red-S-loaded amberlite IRA-400 resin, *Desal., Water Treat.*, 57 (2016) 18551–18559.

- [37] M. Naushad, T. Ahamad, G. Sharma, H. Aláa, A.B. Albadarin, M.M. Alam, Z.A. ALOthman, S.M. Alshehri, A.A. Ghfar, Synthesis and characterization of a new starch/SnO<sub>2</sub> nanocomposite for efficient adsorption of toxic Hg<sup>2+</sup> metal ion, *Chem. Eng. J.*, 300 (2016) 306–316.
- [38] G. Sharma, A. Kumar, S. Sharma, M. Naushad, R.P. Dwivedi, Z.A. ALOthman, G.T. Mola, Novel development of nanoparticles to bimetallic nanoparticles and their composites: a review, *J. King Saud Univ. Sci.*, 2 (2019) 257–269.
- [39] G. Sharma, A. Kumar, M. Naushad, A. Kumar, H. Aláa, P. Dhiman, A.A. Ghfar, F.J. Stadler, M. Khan, Photoremediation of toxic dye from aqueous environment using monometallic and bimetallic quantum dots based nanocomposites, *J. Cleaner Prod.*, 172 (2018) 2919–2930.
- [40] M.T. Islam, A. Dominguez, B. Alvarado-Tenorio, R.A. Bernal, M.O. Montes, J.C. Noveron, Sucrose-mediated fast synthesis of zinc oxide nanoparticles for the photocatalytic degradation of organic pollutants in water, *ACS Omega*, 4 (2019) 6560–6572.
- [41] S. Vijayakumar, B. Vaseeharan, R. Sudhakaran, J. Jayakandan, P. Ramasamy, A. Sonawane, A. Padhi, P. Velusamy, P. Anbu, C. Faggio, Bioinspired zinc oxide nanoparticles using *Lycopersicon esculentum* for antimicrobial and anticancer applications, *J. Cluster Sci.*, 30 (2019) 1465–1479.
- [42] B. Malaikozhundan, B. Vaseeharan, S. Vijayakumar, K. Pandiselvi, M.A.R. Kalanjiam, K. Murugan, G. Benelli, Biological therapeutics of *Pongamia pinnata* coated zinc oxide nanoparticles against clinically important pathogenic bacteria, fungi and MCF-7 breast cancer cells, *Microb. Pathog.*, 104 (2017) 268–277.
- [43] R. Rekha, M. Divya, M. Govindarajan, N.S. Alharbi, S. Kadaikunnan, J.M. Khaled, M.N. Al-Anbr, R. Pavela, B. Vaseeharan, Synthesis and characterization of crustin capped titanium dioxide nanoparticles: Photocatalytic, antibacterial, antifungal and insecticidal activities, *J. Photochem. Photobiol., B*, 199 (2019) 111620.
- [44] N. Serpone, A. Emeline, Semiconductor photocatalysis - past, present, and future outlook, *J. Phys. Chem. Lett.*, 3 (2012) 673–677.
- [45] L. Han, S. Xue, S. Zhao, J. Yan, L. Qian, M. Chen, Biochar supported nanoscale iron particles for the efficient removal of methyl orange dye in aqueous solutions, *PLoS One*, 10 (2015) e0132067.
- [46] J. Fan, Y. Guo, J. Wang, M. Fan, Rapid decolorization of azo dye methyl orange in aqueous solution by nanoscale zerovalent iron particles, *J. Hazard. Mater.*, 166 (2009) 904–910.
- [47] A. Gnanaprakasam, V. Sivakumar, P. Sivayogavalli, M. Thirumarimurugan, Characterization of TiO<sub>2</sub> and ZnO nanoparticles and their applications in photocatalytic degradation of azodyes, *Ecotoxicol. Environ. Saf.*, 121 (2015) 121–125.
- [48] S. Malhotra, Ajowan, *Handbook of Herbs and Spices*, Elsevier, Woodhead Publishing, 2012, pp. 118–137.
- [49] M. Sathishkumar, K. Sneha, Y.-S. Yun, Immobilization of silver nanoparticles synthesized using *Curcuma longa* tuber powder and extract on cotton cloth for bactericidal activity, *Bioresour. Technol.*, 101 (2010) 7958–7965.
- [50] T.Z. Sarmanovna, Phytochemical study of odorous celery root (*Apium graveolens* L.) grown in the north Caucasus, *Pharmacogn. J.*, 11 (2019) 527–530.
- [51] T. Mencherini, A. Cau, G. Bianco, R.D. Loggia, R. Aquino, G. Autore, An extract of *Apium graveolens* var. dulce leaves: structure of the major constituent, apiin, its anti-inflammatory properties, *J. Pharm. Pharmacol.*, 59 (2007) 891–897.
- [52] M. Ovais, A.T. Khalil, A. Raza, M.A. Khan, I. Ahmad, N.U. Islam, M. Saravanan, M.F. Ubaid, M. Ali, Z.K. Shinwari, Green synthesis of silver nanoparticles via plant extracts: beginning a new era in cancer theranostics, *Nanomedicine*, 12 (2016) 3157–3177.
- [53] M. Wang, Y. Zhou, Y. Zhang, S.H. Hahn, E.J. Kim, From Zn(OH)<sub>2</sub> to ZnO: a study on the mechanism of phase transformation, *Cryst. Eng. Comm.*, 13 (2011) 6024–6026.
- [54] B. Sameh, B. Ibtissem, A. Mahmoud, K. Boukef, N.A. Boughattas, Antioxidant activity of *Apium graveolens* extracts, *J. Biol. Active Prod. Nat.*, 1 (2011) 340–343.
- [55] G. Liu, L. Zhuang, D. Song, C. Lu, X. Xu, Isolation, purification, identification of the main phenolic compounds from leaves of celery (*Apium graveolens* L. var. dulce Mill./Pers.). *J. Sep. Sci.*, 40 (2017) 472–479.
- [56] V. Makarov, A. Love, O. Sinityna, S. Makarova, I. Yaminsky, M. Taliansky, N. Kalinina, “Green” nanotechnologies: synthesis of metal nanoparticles using plants, *Acta Nat.*, 6 (2014) 35–44.
- [57] S. Faizi, H. Siddiqi, A. Naz, S. Bano, Specific deuteration in patuletin and related flavonoids via keto–enol tautomerism: solvent- and temperature-dependent <sup>1</sup>H-NMR studies, *Helv. Chim. Acta*, 93 (2010) 466–481.
- [58] T. Rasheed, F. Nabeel, M. Bilal, H.M. Iqbal, Biogenic synthesis and characterization of cobalt oxide nanoparticles for catalytic reduction of direct yellow-142 and methyl orange dyes, *Biocatal. Agric. Biotechnol.*, 19 (2019) 101154.
- [59] T. Khalafi, F. Buazar, K. Ghanemi, Phycosynthesis and enhanced photocatalytic Activity of Zinc oxide Nanoparticles toward organosulfur pollutants, *Sci. Rep.*, 9 (2019) 6866.
- [60] G. Sharmila, C. Muthukumaran, K. Sandiya, S. Santhiya, R.S. Pradeep, N.M. Kumar, N. Suriyanarayanan, M. Thirumarimurugan, Biosynthesis, characterization, and antibacterial activity of zinc oxide nanoparticles derived from *Bauhinia tomentosa* leaf extract, *J. Nanostruct. Chem.*, 8 (2018) 293–299.
- [61] R. Isaac, G. Sakthivel, C. Murthy, Green synthesis of gold and silver nanoparticles using *Averrhoa bilimbi* fruit extract, *J. Nanotechnol.*, 2013 (2013) 906592–906598.
- [62] R. Sathyavathi, M.B. Krishna, S.V. Rao, R. Saritha, D.N. Rao, Biosynthesis of silver nanoparticles using *Coriandrum sativum* leaf extract and their application in nonlinear optics, *Adv. Sci. Lett.*, 3 (2010) 138–143.
- [63] K. Niraimathi, V. Sudha, R. Lavanya, P. Brindha, Biosynthesis of silver nanoparticles using *Alternanthera sessilis* (Linn.) extract and their antimicrobial, antioxidant activities, *Colloids Surf., B*, 102 (2013) 288–291.
- [64] S. Pai, H. Sridevi, T. Varadavenkatesan, R. Vinayagam, R. Selvaraj, Photocatalytic zinc oxide nanoparticles synthesis using *Peltophorum pterocarpum* leaf extract and their characterization, *Optik*, 185 (2019) 248–255.
- [65] T. Varadavenkatesan, E. Lyubchik, S. Pai, A. Pugazhendhi, R. Vinayagam, R. Selvaraj, Photocatalytic degradation of Rhodamine B by zinc oxide nanoparticles synthesized using the leaf extract of *Cyanometra ramiflora*, *J. Photochem. Photobiol., B*, 199 (2019) 111621.
- [66] L. Qin, C. Shing, S. Sawyer, P.S. Dutta, Enhanced ultraviolet sensitivity of zinc oxide nanoparticle photoconductors by surface passivation, *Opt. Mater.*, 33 (2011) 359–362.
- [67] U. Koch, A. Fojtik, H. Weller, A. Henglein, Photochemistry of semiconductor colloids. Preparation of extremely small ZnO particles, fluorescence phenomena and size quantization effects, *Chem. Phys. Lett.*, 122 (1985) 507–510.
- [68] M.M. Khan, N.H. Saadah, M.E. Khan, M.H. Harunsani, A.L. Tan, M.H. Cho, Potentials of *Costus woodsonii* leaf extract in producing narrow band gap ZnO nanoparticles, *Mater. Sci. Semicond. Process.*, 91 (2019) 194–200.
- [69] N. Pantidos, L.E. Horsfall, Biological synthesis of metallic nanoparticles by bacteria, fungi and plants, *J. Nanomed. Nanotechnol.*, 5 (2014) 233–243.
- [70] J. Jiang, G. Oberdörster, A. Elder, R. Gelein, P. Mercer, P. Biswas, Does nanoparticle activity depend upon size and crystal phase?, *Nanotoxicology*, 2 (2008) 33–42.
- [71] J.A. Rodriguez, X. Wang, J.C. Hanson, G. Liu, A. Iglesias-Juez, M. Fernández-García, The behavior of mixed-metal oxides: structural and electronic properties of Ce<sub>1-x</sub>Ca<sub>x</sub>O<sub>2</sub> and Ce<sub>1-x</sub>Ca<sub>x</sub>O<sub>2-y</sub>, *J. Chem. Phys.*, 119 (2003) 5659–5669.
- [72] D. Singh, J. Singh, P. Mishra, R. Tiwari, O. Srivastava, Synthesis, characterization and application of semiconducting oxide (Cu<sub>2</sub>O and ZnO) nanostructures, *Bull. Mater. Sci.*, 31 (2008) 319–325.
- [73] A. Balcha, O.P. Yadav, T. Dey, Photocatalytic degradation of methylene blue dye by zinc oxide nanoparticles obtained from precipitation and sol-gel methods, *Environ. Sci. Pollut. Res.*, 23 (2016) 25485–25493.
- [74] R. Yuvakkumar, J. Suresh, B. Saravanakumar, A.J. Nathanael, S.I. Hong, V. Rajendran, Rambutan peels promoted biomimetic

- synthesis of bioinspired zinc oxide nanochains for biomedical applications, *Spectrochim. Acta, Part A*, 137 (2015) 250–258.
- [75] T. Bhuyan, K. Mishra, M. Khanuja, R. Prasad, A. Varma, Biosynthesis of zinc oxide nanoparticles from *Azadirachta indica* for antibacterial and photocatalytic applications, *Mater. Sci. Semicond. Process.*, 32 (2015) 55–61.
- [76] D. Hu, W. Si, W. Qin, J. Jiao, X. Li, X. Gu, Y. Hao, *Cucurbita pepo* leaf extract induced synthesis of zinc oxide nanoparticles, characterization for the treatment of femoral fracture, *J. Photochem. Photobiol., B*, 195 (2019) 12–16.
- [77] M. Ganesh, S.G. Lee, J. Jayaprakash, M. Mohankumar, H.T. Jang, *Hydnocarpus alpina* Wt extract mediated green synthesis of ZnO nanoparticle and screening of its anti-microbial, free radical scavenging, and photocatalytic activity, *Biocatal. Agric. Biotechnol.*, 19 (2019) 101129.
- [78] R. Vijayalakshmi, V. Rajendran, Synthesis and characterization of nano-TiO<sub>2</sub> via different methods, *Arch. Appl. Sci. Res.*, 4 (2012) 1183–1190.
- [79] S. Sonia, K. Ruckmani, M. Sivakumar, Antimicrobial and antioxidant potentials of biosynthesized colloidal zinc oxide nanoparticles for a fortified cold cream formulation: a potent nanocosmeceutical application, *Mater. Sci. Eng., C*, 79 (2017) 581–589.
- [80] S.T. Fardood, A. Ramazani, S. Moradi, P.A. Asiabi, Green synthesis of zinc oxide nanoparticles using arabic gum and photocatalytic degradation of direct blue 129 dye under visible light, *J. Mater. Sci. - Mater. Electron.*, 28 (2017) 13596–13601.
- [81] H. Agarwal, S.V. Kumar, S. Rajeshkumar, A review on green synthesis of zinc oxide nanoparticles—an eco-friendly approach, *Resour.-Effic. Technol.*, 3 (2017) 406–413.
- [82] C. Vidya, S. Hiremath, M. Chandraprabha, M.L. Antonyraj, I.V. Gopal, A. Jain, K. Bansal, Green synthesis of ZnO nanoparticles by *Calotropis gigantea*, *Int. J. Curr. Eng. Technol.*, 1 (2013) 118–120.
- [83] S.S. Kumar, P. Venkateswarlu, V.R. Rao, G.N. Rao, Synthesis, characterization and optical properties of zinc oxide nanoparticles, *Int. Nano Lett.*, 3 (2013) 30.
- [84] Y.J. Shim, V. Soshnikova, G. Anandapadmanaban, R. Mathiyalagan, Z.E.J. Perez, J. Markus, Y.J. Kim, V. Castro-Aceituno, D.C. Yang, Zinc oxide nanoparticles synthesized by *Suaeda japonica* Makino and their photocatalytic degradation of methylene blue, *Optik*, 182 (2019) 1015–1020.
- [85] A. Jiang, N. Awasthi, A.N. Kolmogorov, W. Setyawan, A. Börjesson, K. Bolton, A.R. Harutyunyan, S. Curtarolo, Theoretical study of the thermal behavior of free and alumina-supported Fe-C nanoparticles, *Phys. Rev. B: Condens. Matter*, 75 (2007) 205426.
- [86] D. Fernandes, R. Silva, A.W. Hechenleitner, E. Radovanovic, M.C. Melo, E.G. Pineda, Synthesis and characterization of ZnO, CuO and a mixed Zn and Cu oxide, *Mater. Chem. Phys.*, 115 (2009) 110–115.
- [87] A. Kołodziejczak-Radzimska, T. Jesionowski, Zinc oxide-from synthesis to application: a review, *Materials*, 7 (2014) 2833–2881.
- [88] K.M. Lee, C.W. Lai, K.S. Ngai, J.C. Juan, Recent developments of zinc oxide based photocatalyst in water treatment technology: a review, *Water Res.*, 88 (2016) 428–448.
- [89] K. Parida, S. Dash, D. Das, Physico-chemical characterization and photocatalytic activity of zinc oxide prepared by various methods, *J. Colloid Interface Sci.*, 298 (2006) 787–793.
- [90] A. Dodd, A. McKinley, M. Saunders, T. Tsuzuki, Effect of particle size on the photocatalytic activity of nanoparticulate zinc oxide, *J. Nanopart. Res.*, 8 (2006) 43–51.
- [91] G. Sharma, V.K. Gupta, S. Agarwal, S. Bhogal, M. Naushad, A. Kumar, F.J. Stadler, Fabrication and characterization of trimetallic nano-photocatalyst for remediation of ampicillin antibiotic, *J. Mol. Liq.*, 260 (2018) 342–350.
- [92] J.M. Coronado, F. Fresno, M.D. Hernández-Alonso, R. Portela, Design of Advanced Photocatalytic Materials for Energy and Environmental Applications, Springer, London, 2013, pp. 123–156.
- [93] Y. Zhang, F. Zhu, J. Zhang, L. Xia, Converting layered zinc acetate nanobelts to one-dimensional structured ZnO nanoparticle aggregates and their photocatalytic activity, *Nanoscale Res. Lett.*, 3 (2008) 201–204.
- [94] D. Chatterjee, V.R. Patnam, A. Sikdar, P. Joshi, R. Misra, N.N. Rao, Kinetics of the decoloration of reactive dyes over visible light-irradiated TiO<sub>2</sub> semiconductor photocatalyst, *J. Hazard. Mater.*, 156 (2008) 435–441.
- [95] M. Guo, M. Fung, F. Fang, X. Chen, A. Ng, A. Djurišić, W. Chan, ZnO and TiO<sub>2</sub> 1D nanostructures for photocatalytic applications, *J. Alloys Compd.*, 509 (2011) 1328–1332.